Moving Fe^{2+} from ferritin ion channels to catalytic OH centers depends on conserved protein cage carboxylates

Rabindra K. Behera[a,1] and Elizabeth C. Theil[a,b,2]

[a]Children's Hospital Oakland Research Institute, Oakland, CA 94609; and [b]Department of Molecular and Structural Biochemistry, North Carolina State University, Raleigh, NC 27695-7622

Edited by Harry B. Gray, California Institute of Technology, Pasadena, CA, and approved April 15, 2014 (received for review September 30, 2013)

Ferritin biominerals are protein-caged metabolic iron concentrates used for iron–protein cofactors and oxidant protection (Fe^{2+} and O_2 sequestration). Fe^{2+} passage through ion channels in the protein cages, like membrane ion channels, required for ferritin biomineral synthesis, is followed by Fe^{2+} substrate movement to ferritin enzyme (F_{ox}) sites. Fe^{2+} and O_2 substrates are coupled via a diferric peroxo (DFP) intermediate, λ_{max} 650 nm, which decays to [Fe^{3+}–O–Fe^{3+}] precursors of caged ferritin biominerals. Structural studies show multiple conformations for conserved, carboxylate residues E136 and E57, which are between ferritin ion channel exits and enzymatic sites, suggesting functional connections. Here we show that E136 and E57 are required for ferritin enzyme activity and thus are functional links between ferritin ion channels and enzymatic sites. DFP formation (K_{cat} and k_{cat}/K_m), DFP decay, and protein-caged hydrated ferric oxide accumulation decreased in ferritin E57A and E136A; saturation required higher Fe^{2+} concentrations. Divalent cations (both ion channel and intracage binding) selectively inhibit ferritin enzyme activity (block Fe^{2+} access), $Mn^{2+} << Co^{2+} < Cu^{2+} < Zn^{2+}$, reflecting metal ion–protein binding stabilities. Fe^{2+}–Cys126 binding in ferritin ion channels, observed as Cu^{2+}–S–Cys126 charge-transfer bands in ferritin E130D UV-vis spectra and resistance to Cu^{2+} inhibition in ferritin C126S, was unpredicted. Identifying E57 and E136 links in Fe^{2+} movement from ferritin ion channels to ferritin enzyme sites completes a bucket brigade that moves external Fe^{2+} into ferritin enzymatic sites. The results clarify Fe^{2+} transport within ferritin and model molecular links between membrane ion channels and cytoplasmic destinations.

iron traffic | oxidoreductase enzyme activity | antioxidant | ferrihydrite | BioIron

Biological and synthetic ion channels transport metal ions through barriers, including those in ferritin protein cages (1–8). How ions reach specific destinations, after exiting ion channels, remains unknown. Ion channels embedded in soluble ferritin protein cages are more accessible to study than membrane ion channels embedded in lipid-rich membranes. Fe^{2+} substrate is transported into ferritin protein cages through multiple ion channels that penetrate the cages (Fig. 1 *A*–*D*) and is delivered to multiple ferritin enzyme (F_{ox}) sites. Each ferritin enzyme site binds 2 Fe^{2+} substrate ions which, in eukaryotic ferritins, react with O_2 substrate; the intermediate of enzyme activity is diferric peroxo (DFP) that decays to diferric oxy, the precursors of protein-caged ferritin biominerals ($Fe_2O_3{\cdot}H_2O$). Ferritin biominerals vary in size, depending on iron availability, up to 4,500 Fe/cage. Rapid (ms) formation of blue color DFP (λ_{max}: 650 nm) (9, 10) requires cooperative binding of 2 Fe^{2+}/active site (Hill coefficient = 3) (11) and indicates correct Fe^{2+} delivery to the multiple ferritin enzymatic centers. Ferritin protein-caged iron biominerals, slow to dissolve in solution (Fig. S1), are metabolic iron concentrates for cofactor biosynthesis such as heme or iron-sulfur clusters. The conversion of Fe^{2+} and O_2 into protein-coated solids inside ferritin cages is an antioxidant activity, and ferritin genes are regulated with other antioxidant response proteins (4, 12, 13).

Ferritin protein ion channels are 15 Å long, analogous to short ion channels in biological membranes (3). Positioned around the threefold symmetry axes of the cage (Fig. 1), ferritin protein ion channels form during cage self-assembly from three proximal subunits; ion channel amino acids are highly conserved (Table 1) (14). Both external and internal ferritin ion channel pores are 4–5 Å in diameter with a midchannel constriction, 2.3 Å in diameter, created by the carboxylate side chains from the three glutamate residues at position 130. In protein crystals, ferritin ion channels bind a variety of divalent metal ions (Fig. S2*B* and Table S1). Because hydrated ions have diameters of 6.4–6.9 Å, partial dehydration must occur for ion passage through the E130 constriction (2.3-Å diameter). Only single metal atoms are observed in protein–metal crystal structures at the ring of three E130 residues, contrasting with the multiple metal atoms accumulated near the channel exits around the ring of three D127 residues with shorter carboxylate side chains (Fig. 1 *B* and *C*); multiple ordered water molecules also accumulate near D127.

Here we report functional studies that trace the movement of Fe^{2+} from ferritin ion channel exits to ferritin enzyme sites (Fig. 1). The strategy is to compare enzymatic reactions among variant ferritins E57A, E136A, and E57A/E136A to WT and to an ion channel variant, E130D, which has detectable enzymatic activity; in protein crystal structures, ferritin cage residues E57 and E136 have multiple conformations and bind metal ions. Enzymatically active ferritin subunits (type H) in eukaryotic ferritin couple Fe^{2+}

Significance

How ions move between ion channel exits and final destinations is poorly understood. Fe^{2+} substrate enters ferritin protein nanocages through cage-penetrating ion channels analogous to membrane ion channels. Fe^{2+} then moves to ferritin cage enzyme (F_{ox}) sites, reacting with oxygen substrate to produce diferric oxy complexes, the precursors of ferritin minerals ($Fe_2O_3{\cdot}H_2O$). Ferritin iron is used in heme and iron–sulfur cofactors. Monitoring rapid (ms) diferric peroxo formation in WT ferritin and E57 and E136 variants showed that these conserved residues are required for enzyme activity. Combining the results with older structural studies identifies ferritin E57 and E136 links in the Fe^{2+} bucket brigade connecting ferritin ion channels and destinations. By analogy, key carboxylates in ion transporters link ion channels to cytoplasmic destinations.

Author contributions: R.K.B. and E.C.T. designed research; R.K.B. performed research; R.K.B. and E.C.T. analyzed data; and R.K.B. and E.C.T. wrote the paper.

The authors declare no conflict of interest.

This article is a PNAS Direct Submission.

[1]Present address: Department of Chemistry, National Institute of Technology, Rourkela 769008, Odisha, India.

[2]To whom correspondence should be addressed. E-mail: etheil@chori.org.

This article contains supporting information at www.pnas.org/lookup/suppl/doi:10.1073/pnas.1318417111/-/DCSupplemental.

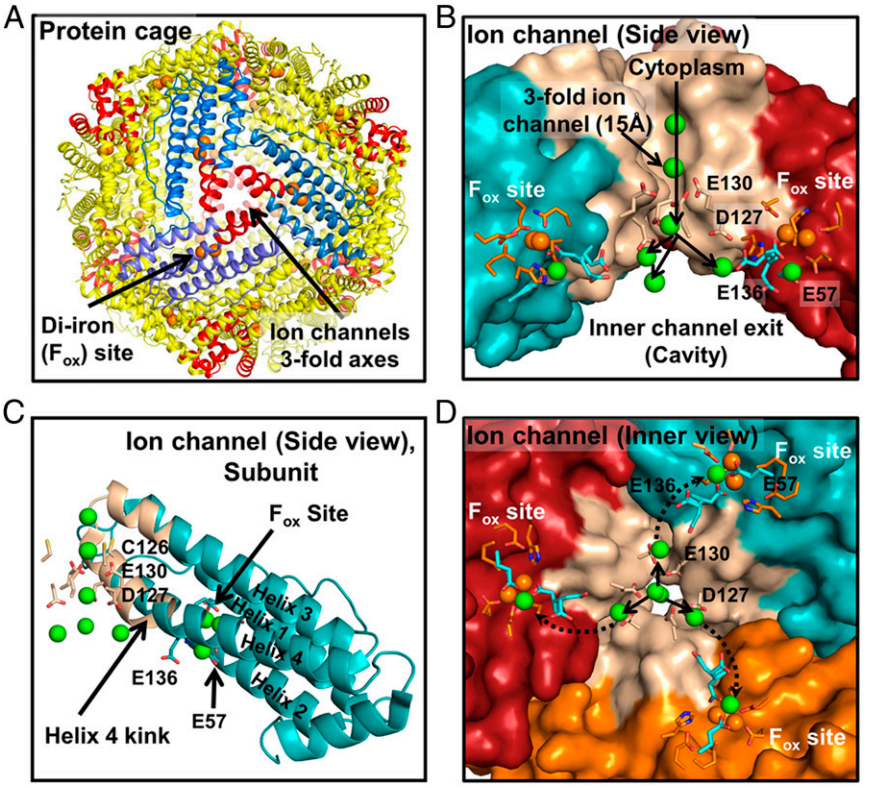

Fig. 1. Ion channels in soluble ferritin protein nanocages transport Fe^{2+} to multiple catalytic centers (F_{ox} or oxidoreductase sites). (*A*) The 24-subunit ferritin protein cage. Red helices, Fe^{2+} channels. (*B*) A ferritin Fe^{2+} ion channel (side view). Green spheres, metal ions. Conserved residues E57 and E136 are putative carboxylate links in Fe^{2+} transit between ferritin ion channel carboxylate (E130 and D127) and ferritin enzyme (F_{ox}) sites based on phylogenetic structural location and conformational flexibility in protein crystals (16, 18). (*C*) A single ferritin protein cage subunit (side view). Tan, channel helix segments. (*D*) Ion channel (viewed from inside the protein cage). Green spheres, metal ions. Prepared from PDB 3KA3 using PyMol.

and O_2 substrates in an oxidoreductase reaction that may be written as

$$2\left[Fe^{2+}\bullet H_2O\right] + O_2 \rightarrow \left[(H_2O\bullet Fe^{3+}\text{-O-O-}\ Fe^{3+}\bullet H_2O)\right] \rightarrow Fe_2O_3 \bullet H_2O + 4H^+.$$

A blue diferric peroxo intermediate forms in ms and decays quickly (<1 s) (4, 12, 13). Diferric oxy enzymatic reaction products in ferritin are released inside the protein cage and coalesce into ferric-oxo multimers within nucleation channels between the enzyme sites and the central mineral growth cavity (Fig. 1); stoichiometric amounts of hydrogen peroxide and Fe^{3+} are detected at subsaturating amounts of Fe^{2+} (<36 Fe/cage). Sets of four proximal nucleation channel exits surround the inner surface of the fourfold cage axes, which can facilitate ordered interactions among the emerging biomineral precursors (8). Engineered ferritin variants E57A and E136A lack the conserved carboxylate residues that lie between the ion channel exits and the diiron enzymatic sites. Ferritin E130D ion channels were designed to compare an enzymatically active ion channel variant ferritin with cage variants E57A and E136A. Ferritin variants E130A and D127, characterized earlier (14, 15), had little or no detectable enzyme activity. The results show the crucial roles of E136 and E57 in ferritin Fe^{2+} traffic within ferritin protein cages: (*i*) Loss of enzymatic activity in ferritin variants E136A and E57A indicated a role in delivering Fe^{2+} substrate to interior enzymatic sites. (*ii*) Ion channel and transfer site binding metal ions inhibited ferritin enzymatic activity selectively (Mn^{2+} << Co^{2+} < Cu^{2+} < Zn^{2+}). (*iii*) Metal ion binding at ferritin ion channel Cys126 residue (forming Cu–S charge transfer complex) indicates that metal ion coordination to sulfur can complement ionic binding during Fe^{2+} transit through ion channels.

Results

Conserved Carboxylates E57 and E136 Are Required for Rapid Reactions of Fe^{2+} at Ferritin Enzyme Centers. Ferritin variants E57A and E136A (Fig. 1*C*) (16, 17) were constructed for the following reasons: (*i*) E57 and E136 are highly conserved, (*ii*) E57 and E136 lie between internal exits and diiron catalytic centers (Table S1)

Table 1. Conservation of ferritin amino acids in Fe^{2+} cage transfer residues and ion channel walls

Organism	Transfer carboxylates: E136 and E57	Ion channel: helix 4
	Eukaryotes	
Frog M	HSHEEREHAE–EEQVKDIK	DPHLCDFLESEYL
Frog H	QSHEEREHAE–EEQVKSIK	DPHLCDFLETEYL
Human H	QSHEEREHAE–NEQVKAIK	DPHLCDFIETHYL
Human L	LAEEKREGYE–DEEVKLIK	DPHLCDFLETHFL
Human Mt-H	QSREETEHAE–NEQVKSIK	DPHLCDFLETYYL
Horse H	QSHEEREHAE–NEQVKAIK	DPHLCDFLETHYL
Rabbit H	QSHEEREHAE–NEQVKSIK	DPHLCDFIETHYL
Mouse H	QSHEEREHAE–SEQVKSIK	DPHLCDFIETYYL
Soybean H	SSEEEREHAE–GEQVEAIK	DVQLADFVETEYL
Maize H	SSDEEREHAE–EEQGEAIN	DPQLTDFIESEFL
	Bacteria	
E. coli-BFR	ESIDEMKHAD–DEEGHIDW	DYVSRDMMIEILR
E. coli-FTNA	HAQEEMTHMQ–SEQHEEEK	DYPTFNFLQ-WYV

Underlined, Fe^{2+}. Transfer carboxylates: E57 and E136. Ion channels walls in helix 4, residue numbers 122–134. Ferritin sequence conservation among eukaryotic ferritins is high, whether in the cytoplasm (animals), plastids (plants), or mitochondria (Mt).

(16–19), (*iii*) E57 and E136 bind metal ions in ferritin protein crystals (Table S1) (16–19), and (*iv*) E57 and E136 assume multiple conformations in ferritin protein crystals (16, 18). E136 carboxylates point either toward channel carboxylates or toward E57, and E57 carboxylates point either toward one of the E136 conformations or toward ferritin enzyme site carboxylate E58. Structurally, ferritin contains a chain of ion channel carboxylates extending through the cage-penetrating ion channels and the protein cage to the catalytic centers. The variant ferritins behaved as WT in native gel electrophoresis, normal disassembly/unfolding in SDS gel electrophoresis and during Q-Sepharose (anion exchanger) chromatography, indicating normal cage assembly and surface charge.

DFP formation and decay (Fig. 2*A* and Tables S2 and S3) was inhibited in ferritin E57A, E136A, and E57A/E136A; k_{cat}/K_m decreased (Fig. 2*B* and Table S2). Effects in ferritin E57A were larger than in ferritin E136A, but the largest inhibition was in ferritin E57A/E136A, where k_{cat}/K_m decreased by ∼20-fold (Table S2). Greater inhibition in ferritin E57A compared with ferritin E136A was observed, possibly because E57 is closer to the active site and bridging ligand E58 or due to charge neutralization for E136 by conserved neighbors K139. In the ferritin double variant, the V_{max} for DFP formation required 1,180 Fe/cage (or 49 Fe/enzyme site) compared with 197 Fe/cage (or 8 Fe/enzyme site) in WT (Fig. 2*B* and Table S2). The sixfold increase in Fe^{2+} concentrations required to saturate ferritin enzyme sites in variant ferritins E136A and E57A indicates the importance of the two carboxylate residues in directing Fe^{2+} from ferritin ion channels to ferritin enzyme sites.

Ferritin E57 and E136 Contribute to Multiple Enzymatic Turnovers and Mineral Nucleation. Ferritins are distinct from other multisite enzymes because the catalytic products do not move far away; instead, they remain inside the protein cage, albeit at different locations (20–22). Because experiments with 48 Fe/protein cage (2 Fe^{2+} substrate/enzyme site, the amount required to reach maximum DFP formation in empty ferritin protein cages) might only examine priming effects, higher iron concentrations were analyzed (>2 Fe^{2+}/enzyme site). When 480 Fe^{2+} are added per protein cage (20 Fe^{2+}/enzyme site) to increase DFP decay in WT ∼threefold, DFP decay barely changed in E57A, E136A, and E57A/E136A ferritins (Fig. 2*C* and Table S4) (Fig. 2 and Tables S2–S4). However, replacing an ion channel carboxylate such as D122 near the external surface of ferritin cages alters both Fe^{2+} entry and exit rates (14). The more general effect of D122 substitution contrasts with the selectivity of changing cage residues E57 and E136 that only affect Fe^{2+} substrate entry/enzyme activity (Fig. 2 and Tables S2–S4).

The roles of ferritin cage residues E57 and E136 in directing ferritin iron traffic extended beyond enzymatic coupling of 2 Fe^{2+} with O_2 at the catalytic centers to bulk biomineral growth. Bulk mineral grows in the central cavity of ferritin protein cages, after iron moves through the ion channels, past residues E136 and E57, through the catalytic centers and through the 20-Å protein channels, where $[Fe^{3+}O]_x$ nucleation begins (8, 15, 20). Growth of the caged ferritin iron biominerals was inhibited 80% in ferritins E57A and E136A (Fig. 2*D*), in addition to inhibition of $2Fe^{2+}/O_2$ catalysis (Fig. 2*A*), indicating coordination of functions throughout ferritin protein cages.

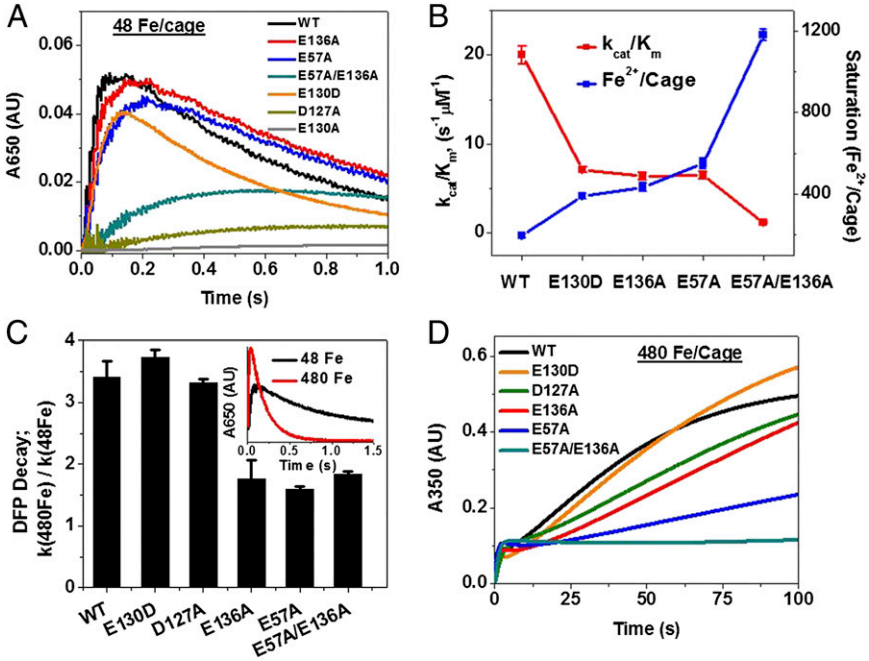

Fig. 2. Residues E57 and E136 are required for rapid access of Fe^{2+} substrate to ferritin catalytic sites for DFP formation as well as biomineralization. (*A*) Progress curves: diferric peroxo (DFP) catalytic intermediate, 48 Fe^{2+}/cage (2 Fe^{2+}/subunit) ($A_{650\ nm}$). Ferritins E130A and D127A characterized earlier (14, 15) are analyzed here for comparison with E57A and E136A. (*B*) Catalytic efficiency (k_{cat}/K_m) and Fe^{2+} saturation of ferritin enzyme sites that oxidize 2 Fe^{2+}(DFP formation). (*C*) Stabililzation of DFP at high iron:protein ratios (480 Fe^{2+}/cage) in E57A, E136A, and E57A/E136A variant ferritins. (*D*) E57A and E136A inhibition of $[Fe^{3+}O]_x$ (biomineral) growth ($A_{350\ nm}$) compared with WT. D127, E130, ion channel residues; E136, E57, flexible cage transfer residues. Concentrations of ferritin in solution (0.1 M Mops·Na, 0.1 M NaCl, pH 7.0) were (*A* and *C*) 50 μM, subunits (2.08 μM, protein cages); (*B* and *D*) 25 μM, subunits (1.04 μM, protein cages). Protein solutions, rapidly mixed (<5 ms) with fresh, acidic solutions of $FeSO_4$, were analyzed by UV-vis spectroscopy at 350 and 650 nm, as previously described. The data are averages of three to four independent experiments, using two different independent protein preparations for each protein; the error is the SD. Note the large differences in time scales for *A* (0–1 s, $A_{650\ nm}$) and *D* (0–100 s, $A_{350\ nm}$); in *C* the stabilization of DFP compared with WT and ion channel variants E130D and D127A, and in *D*, caged biomineral growth was faster in WT and ion channel ferritin variants E130D and D127A than in ferritin cage transfer residue variants E136A and E57A.

Divalent Metal Ion Binding to Ferritin Protein. Ferritin crystal structure either cocrystallized or soaked with divalent metal ions shows metal ion binding sites at least at three places: along the threefold channels, at the intracage transit site residues E57 and E136, and at diiron catalytic sites. To determine if these divalent metal ions could alter the delivery of Fe^{2+} substrate to ferritin enzyme sites, we studied the effects of Zn^{2+}, Cu^{2+}, Co^{2+}, and Mn^{2+} on diferric peroxo formation in WT ferritin. Zn^{2+} and Cu^{2+} were the more effective inhibitors of ferritin enzyme activity and mineral growth (Fig. 3 *A* and *B*). Co^{2+} was only 12% as effective an inhibitor as Zn^{2+}, but 400% more effective than Mn^{2+} (Table S5 and Fig. S2*A*). In general, the differences reflect different metal–protein stabilities. Metal ion inhibition in ferritin variants E57A and E136A was so great in single experiments that reliable numbers were difficult to obtain, and they were not studied further. The stronger inhibition in ferritin E57A/E136A suggests that in the absence of intracage transit site residues, Fe^{2+} will face stronger resistance to cross the internal gate (57A and 136A) and also need to replace already bound metal inhibitors from the F_{ox} site for the catalytic oxidation.

Activity of ferritin E130D, an ion channel variant, against which ferritin transfer residue variants (E57A and E136A) could be compared, was examined with the same series of metal ions. Very low activity in ferritin ion channel variants, such as E130A and D127A, required the construction of ion channel variant ferritin E130D, which has significant, albeit decreased, activity. Solutions of ferritin E130D also had an unpredicted feature. Although solutions of WT are relatively colorless when Cu^{2+} is added, ferritin E130D forms a stable, blue-green color when Cu^{2+} is added (Fig. 3*D*). By contrast, solutions of ferritin WT and ferritin E57A or E136A were relatively colorless when Cu^{2+} was added. The UV-vis spectra of Cu-E130D ferritin solutions indicate a Cu–S protein charge transfer complex. Fortuitously, there is only one cysteine; channel identification of the ferritin protein cysteine residues in the Cu complex as C126. Such observations suggest that in WT ferritin, transient Fe–S interactions occur. Involvement of C126 in ferritin function was suggested more than 20 y ago, as a change in ferritin function (Fe^{2+} oxidation) when the ferritin C126-SH side chain was alkylated (23). Thus, two types of experimental observations support a transient Fe^{2+}–S interaction in ferritin ion channels during Fe^{2+} transit: (*i*) Fe^{2+} oxidation rates change in ferritin when C126 was alkylated (23) and (*ii*) modification of ion channel properties, as in ferritin E130D, changes ferritin enzyme activity.

A direct test of C126 function in ferritin used ferritin C126 S where the –SH in channel residue cysteine 126 was converted to –OH (serine 126) by protein engineering (recombinant DNA and protein expression technologies). In ferritin C126S, ferritin enzyme activity increased: C126S/WT = 2.3 ± 04. Such an observation supports a role for Fe^{2+}–C126–SH in binding/selectivity of Fe^{2+} entering ferritin protein cages. Thus, the three sulfhydryl groups from the three C126 residues near the ferritin ion channel exterior entrance appear to pull Fe^{2+} into the ion channel, and the ring of three E130 carboxylates in midchannel pulls Fe^{2+} through to the three D127 carboxylates near the internal channel exits; here clusters of metal ions are observed, suggesting distribution to the three nearby E136 cage residues in each of the three subunits that form the ion channels (Fig. 4).

Discussion

The activity of ferritin protein cage transfer residues E136 and E57 reported here identifies the functional links between the ion channel exits and the enzyme site destinations. E57 and E136 contribute to at least two different components of ferritin catalysis: (*i*) facilitating Fe^{2+} binding at catalytic sites, as illustrated by the smaller number of Fe^{2+} required for saturation [WT, 8 Fe/subunit vs. E136A or E57A, 20–50 Fe/subunit (Fig. 2*B*)] and (*ii*) promoting diferric peroxo intermediate decay and facilitating

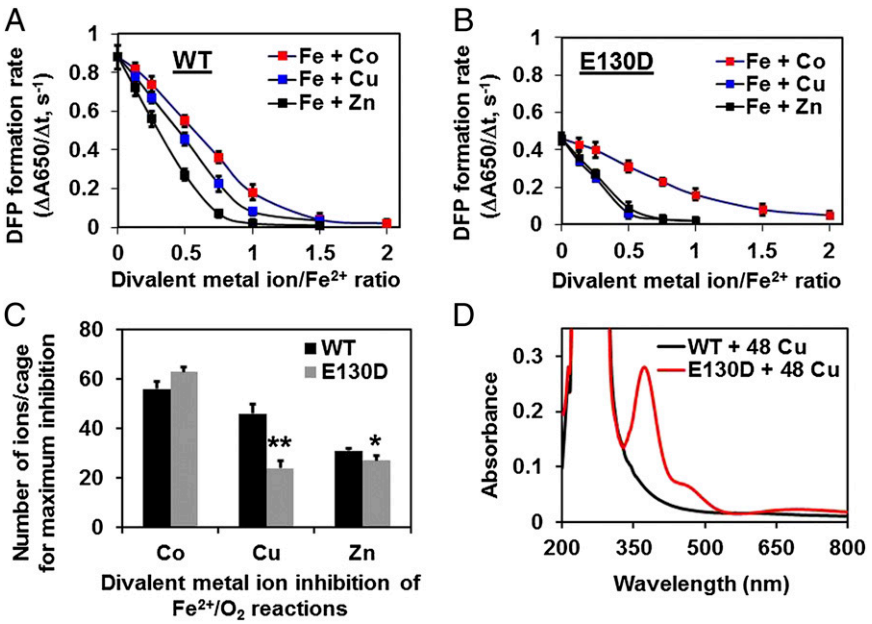

Fig. 3. Selective effects of Co^{2+}, Cu^{2+}, and Zn^{2+} on ferritin activity. Solutions of metal cation inhibitors Co^{2+}, Cu^{2+}, or Zn^{2+} (6–96 metal ions/protein cage) were added to ferritin protein cage solutions in 0.2 M Mops·Na, 0.2 M NaCl, pH 7.0, for 1 h, before rapidly mixing (<5 ms) with acidic solutions of $FeSO_4$ (48 Fe^{2+}/cage) at 25 °C; final protein concentrations were 50 μM, subunits (2.04 μM, protein cages). (*A* and *B*) Effects of Co^{2+}, Cu^{2+}, and Zn^{2+} on $2Fe^{2+}/O_2$ catalysis (diferric peroxo, $A_{650\ nm}$, formation): (*A*) WT and (*B*) E130D. (*C*) Comparisons of metal cation inhibition in WT and E130D ferritin at 48 Fe/cage (2 Fe/enzyme site). Data for ferritin E130D with Cu^{2+} and Zn^{2+} were significantly different from WT: $^*P < 0.01$; $^{**}P < 0.001$. The inhibition of enzyme activity by metal cations in *A* of ferritins E136A and E57A/E136A was so great that reliable measurements were not possible. (*D*) Differences in UV-vis spectrum of Cu^{2+}-WT ferritin and Cu^{2+}-E130D ferritin. The spectrum of Cu^{2+}-E130D ferritin is of a Cu–Cys charge transfer complex. The data in *A*–*C* are averages (±SD). All data are from two to four independent experiments, using two to three different protein preparations of each protein.

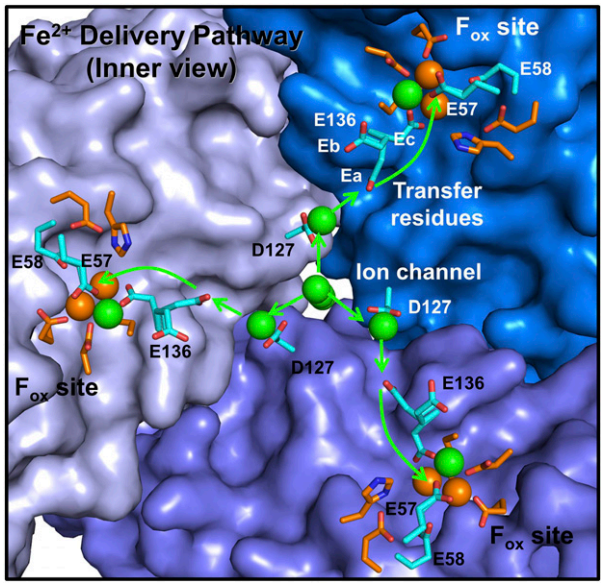

Fig. 4. The Fe^{2+} bucket brigade that moves Fe^{2+} into ferritin protein cages. Three enzyme sites for the reaction of 2 Fe^{2+} with O_2 (rust) are shown in the three subunits that form one of the ion channels into a ferritin protein cage; in a 24-subunit eukaryotic ferritin, as studied here, there are eight ion channels and 24 enzyme sites (1/subunit). Green arrows show the path taken by entering Fe^{2+} through an ion channel to three enzyme sites in a ferritin protein cage, based on the results here. [The enzyme sites are also called ferroxidase (F_{ox}) sites or oxidoreductase sites.] F_{ox} site residues are E23, E58, H61, E103, Q137, and D140, described in ref. 28; D140 can also be S140 or A140 in different eukaryotic ferritins, but in eukaryotic ferritins, residue 140 is never H (29), as it would be in a diiron cofactor. Q137 is a specific and conserved characteristic of eukaryotic ferritin enzyme sites (28). The multiple conformations of E136 and E57 observed in ferritin protein crystals (16, 18) are shown only for E136 for simplicity: 136_a, 136_b, and 136_c. The multiple conformations of E57, which are omitted, point either toward one of the E136 conformations or toward active site E58. Each of the three cage subunits contributing to the ion channel walls are drawn in different shades of blue. Residues in the Fe^{2+} bucket brigade are blue; O atoms are red. Colored spheres: green, multiple metal ions aligned down the middle of the ion channel, clustered at the D127 ring and en route to the catalytic sites; rust, Fe^{2+} at the ferritin di-Fe^{2+} enzyme centers.

postoxidation biomineralization (Fig. 2 *C* and *D* and Table S4). The multiple conformations of E136 and E57, which have been observed in protein crystals (14, 18), can facilitate rapid Fe^{2+} delivery from ion channels to diiron catalytic sites. E136 points either toward the ion channel exit or toward E57, and E57 points either toward E136 or toward active site E58 residue, which bridges two Fe^{2+} substrate ions when they are bound in a ferritin enzyme site. The ferritin cage residues E136 and E57 thus complete a bucket brigade that rapidly moves Fe^{2+} from the external environment through the ion channels to the enzyme sites in ferritin protein cages (Fig. 4).

Fe^{2+} reaches the multiple enzyme sites buried in the ferritin protein cage in <10 ms, after traveling 28 Å through the ion channels and the cage itself. The ion channel constriction created by three E130 residues tolerates neither shortening carboxylates, as in ferritin E130D where catalysis is slowed (DFP formation decreased by 80% and k_{cat}/K_m decreased by 65%; Table S3), nor replacing –COOH side chains with $–CH_3$ as in E130A (DFP is undetectable) (17). In small (12-subunit) ferritins, also called Dps proteins, negative ion channel electrostatics are created by a ring of carboxylates that are critical for Fe^{2+} transit (6, 23, 24). The E130D ferritin variant in a large (24-subunit) ferritin described here emphasizes the importance of localized –ve charge density in all ferritin ion channels, large and small, for pulling Fe^{2+} through the ion channels toward transit cage residues.

An unpredicted feature of Fe^{2+} movement through ferritin ion channels observed here was S complexation with channel residue C126 near the external entrance of the channels, revealed by the stable Cys–Cu^{2+} complex in E130D ferritin (Fig. 3 *C* and *D*). Models of metal ion inhibition often focus on competition for Fe^{2+} between protein binding sites, both ion channels and catalytic centers, and on the stability of metal–O or metal–N binding. In such models, inhibition is $Zn^{2+} > Cu^{2+} > Co^{2+} > Mn^{2+}$ and follows the Irving Williams series for metal–protein stability discussed in ref. 25, except that Cu^{2+} shows less inhibitory effect than Zn^{2+}. Although inhibition of both WT and E130D variant ferritins shares with other proteins the relationships between metal ion and activity inhibition (Fig. 3 and Table S1), the newly observed Cu–Cys charge transfer complex in ferritin E130D (Fig. 3*D*) requires a divergent model where Fe^{2+} ions bind coordinately to an ion channel cysteine. The inhibitory effects of cysteine alkylation in horse spleen ferritin observed decades ago (26) can now be explained by Fe^{2+}–Cys126 interactions in normal ferritin ion channels; Fe^{2+}–Cys complexes are relatively common in proteins (26).

However, Cys126, present only in the ion channels of animal ferritins (Table 1), explains the generally faster iron oxidation kinetics in animal ferritins (15) and likely contributes to the toxicity of copper in animals, including humans. Inner sphere complexation (Fe–S–Cys), electrostatics (carboxylate chain), and geometry (channel shape and diameter) all appear to contribute to Fe^{2+} transit, at least in ion channels of animal ferritins.

The new results explain the observation that Fe^{2+} binds randomly to each of the two Fe^{2+} sites in ferritin enzyme centers (11). In one conformation, E57 points toward E58; E58 bridges two Fe^{2+} substrate ions in ferritin enzyme sites. Thus, E58 carboxylate is a ligand to both diiron catalytic sites (Fe1 and Fe2). E57 delivers Fe^{2+} to the diiron catalytic site, and iron is delivered to each site within the diiron catalytic centers with equal probability. As an ancient protein, nature has had billions of years to optimize ferritin protein cage structure and function to the complexity of extant ferritin protein nanocages. Considering the parsimony of nature, analogous ion transfer paths likely exist for membrane ion channel proteins. Such paths are needed to link ion traffic through membrane ion channels to cytoplasmic destinations in physiological processes such as intracellular cation balance (27). Finding the molecular links between membrane ion channels and destinations in living cells and exploiting them for directed ion traffic and protein cage nanotechnology are future directions.

Materials and Methods

Preparation of Recombinant Ferritins. Ferritin variants were constructed in the well-characterized frog ferritin M WT protein encoded in pET-3a vector by using QuikChange Mutagenesis (Stratagene) Kit (28, 29). Primers used for site-specific mutagenesis were the following: E130D forward: 5′-CATCTGTGTGATTTCCTGGATTCTGAATATCTGGAGGAA-3′; E130D reverse: 5′-TTCCTCCAGATATTCAGAATCCAGGAAATCACACAGATG-3′; C126S forward: 5′- AAGTTGACCCCCATCTGAGTGATTTCCTGGAATCT-3′; C126S reverse: 5′-CCAGGAAATC-ACTCAGATGGGGGTCAACTT-3′; E136A forward: 5′-GGAATCTGAATATCTGGAGGCACAG-GTGAAGG-3′; E136A reverse: 5′-CCTTCACCTGTGCCTCCAGATATTCAGATTCC-3′; E57A forward: 5′-GGAGCACAGTCATGCGGAGAGGGAGCATG-3′; E57A reverse: 5′-CATGCT-CCCTCTCCGCATGACTGTGCTCC-3′. Ferritin D127A plasmid has been described elsewhere (15). The double mutant, E57A/E136A, was prepared with the E57A template and E136A primers.

WT and the variant ferritins were expressed in *Escherichia coli* BL21(DE3) pLysS (Stratagene) and were purified from washed cells that were lysed by sonication; lysates heated to 65 °C for 15 min were clarified by sedimentation at 19,000 × *g*, followed by precipitation with ammonium sulfate, dissolution, and dialysis to remove salt and exchange buffers. Proteins were resolved by Q-Sepharose chromatography, as previously described (28); variant ferritins behaved like WT. Betaine and sorbitol, added to bacterial culture medium, increased yields (28) of recombinant ferritin E57A or E57A/E136A. Protein concentrations were measured by the Bradford assay and the iron

content (<7 Fe/molecule of assembled protein cages) as the Fe^{2+}-1,10-phenanthrolene or ferrozine complex.

Kinetics of Ferritin Fe^{2+}/O_2 Oxidoreduction Catalysis. Fe^{2+} substrate was added, in air, at concentrations equivalent to 48 Fe^{2+}/ferritin protein cage (2 Fe^{2+}/ferritin enzyme site) for single-turnover conditions; up to 480 Fe^{2+}/cage (20 Fe^{2+}/ferritin enzyme site) was used for multiple-turnover conditions (9, 10). Buffered solutions of recombinant proteins were rapidly mixed (<5 ms) with freshly prepared solutions of $FeSO_4$ in 1.0 mM HCl (29), at 20 °C in a stopped-flow UV-vis spectrophotometer (Applied Photophysics). The catalytic intermediate, diferric peroxo, was monitored at 650 nm, the λ_{max} for the transient DFP intermediate (9, 10). Final concentrations of ferritin protein cages were 2.08 and 1.04 μM for 48 Fe and 480 Fe/24 subunit ferritin protein cage, respectively, in 0.1 M Mops·Na, pH 7.0, and 0.1 M NaCl; when very high iron:protein ratios were analyzed, the buffer was 0.2 M Mops·Na and 0.2 M NaCl at pH 7.0.

For saturation kinetics, equal volumes of proteins solutions were mixed with freshly prepared solutions of $FeSO_4$, 0.025–3 mM, in 1.0 mM HCl, at 20 °C, in a stopped-flow spectrophotometer. The general analytical approaches were developed earlier as described in refs. 28 and 29. Absorbance changes were recorded at 650 and 350 nm. The observed initial rates (V_i) (linear phase), plotted as function of varying Fe^{2+} concentrations, were fit to the Hill (sigmoidal/growth) equation $[V_i = V_{max}[Fe^{2+}]^n/(K_m)^n + [Fe^{2+}]^n]$ using Origin 8.0 Pro, to obtain parameters obtained for saturation kinetics and the Hill coefficient for DFP and $[Fe^{3+}–O]_x$ species.

Metal Ion Inhibition of Ferritin Catalysis. The potential metal ion inhibitors $MgSO_4$, $CaSO_4$, $MnSO_4$, $CoSO_4$, $CuSO_4$, or $ZnSO_4$ were added to 4.16 μM ferritin protein solutions in 0.2 M Mops·Na and 0.2 M NaCl at pH 7.0 and preincubated for 1.0 h at room temperature before monitoring DFP formation by adding Fe^{2+} (48/cage) to it. Final concentration of ferritin protein was 2.08 μM in 0.1 M Mops, pH 7.0, 0.1 M NaCl. Initial rates were obtained as described in the saturation kinetics section.

Mineral Formation in Ferritin. Changes in the absorbance at 350 nm ($A_{350\ nm}$), a midpoint in the broad absorbance bands of $[Fe^{3+}\text{-}O]_x$ species (DFP formation, diferric oxo formation, ferric oxo nucleation, and mineralization/bulk $Fe_2O_3{\cdot}H_2O$ formation), were monitored; some investigators monitor changes at 310 or 420 nm, instead. UV-vis spectral resolution of the multiple ferric species has not yet been achieved contrasting with the early intermediate, DFP. However, DFP is present only for 1 s after mixing, in contrast with $A_{350\ nm}$, where absorbance changes continue for more than 2 h. Ferritin samples were incubated for 2 h at room temperature after mixing with Fe^{2+} in air and finally stored at 4 °C and were analyzed for mineral dissolution rates after 24 h (14, 15).

Mineral Dissolution in Ferritins (Fe^{2+} Exit). Ferritin protein with caged minerals of $Fe_2O_3{\cdot}H_2O$ (Fe = 480/cage) were prepared by adding solutions of ferrous sulfate to solutions of empty protein cages in 100 mM Mops pH 7.0 containing 100 mM NaCl, as previously described (17). Mineral dissolution and Fe^{2+} exit were monitored at 522 nm, the absorbance maximum of Fe^{2+}-(2, 2′-bipyridyl)$_3$, after reduction of ferric minerals. The caged $Fe_2O_3{\cdot}H_2O$ was reduced by a mixture of NADH and FMN, which was added to a solution of 0.5 μM mineralized ferritin (0.25 mM Fe) containing 2.5 mM bipyridyl at 25 °C; the final concentrations of NADH and FMN were 2.5 mM. The percentages of Fe^{2+} exit after 2 h were calculated from the absorbance changes at 522 nm, the iron concentration (0.25 mM), and the extinction coefficient (ε_{522} = 8.34 $mM^{-1}{\cdot}cm^{-1}$) for the Fe^{2+}–(2,2′-bipyridyl)$_3$ complex. The data were averaged from a minimum of four experiments using a minimum of two independent protein preparations.

ACKNOWLEDGMENTS. We thank Caroline D. Lee and Yekuri Sekune for technical assistance and Dr. Takehiko Tosha for helpful discussions. This work was supported by Children's Hospital Oakland Research Institute Partners and National Institutes of Health Grant DK20251.

1. Gouaux E, Mackinnon R (2005) Principles of selective ion transport in channels and pumps. *Science* 310(5753):1461–1465.
2. Richards LA, Schäfer AI, Richards BS, Corry B (2012) The importance of dehydration in determining ion transport in narrow pores. *Small* 8(11):1701–1709.
3. Corringer PJ, et al. (2012) Structure and pharmacology of pentameric receptor channels: From bacteria to brain. *Structure* 20(6):941–956.
4. Liu X, Theil EC (2005) Ferritins: Dynamic management of biological iron and oxygen chemistry. *Acc Chem Res* 38(3):167–175.
5. Takahashi T, Kuyucak S (2003) Functional properties of threefold and fourfold channels in ferritin deduced from electrostatic calculations. *Biophys J* 84(4): 2256–2263.
6. Ceci P, et al. (2011) Effect of the charge distribution along the "ferritin-like" pores of the proteins from the Dps family on the iron incorporation process. *J Biol Inorg Chem* 16(6):869–880.
7. Douglas T, Ripoll DR (1998) Calculated electrostatic gradients in recombinant human H-chain ferritin. *Protein Sci* 7(5):1083–1091.
8. Theil EC (2011) Ferritin protein nanocages use ion channels, catalytic sites, and nucleation channels to manage iron/oxygen chemistry. *Curr Opin Chem Biol* 15(2): 304–311.
9. Treffry A, Zhao Z, Quail MA, Guest JR, Harrison PM (1995) Iron(II) oxidation by H chain ferritin: Evidence from site-directed mutagenesis that a transient blue species is formed at the dinuclear iron center. *Biochemistry* 34(46):15204–15213.
10. Pereira AS, et al. (1998) Direct spectroscopic and kinetic evidence for the involvement of a peroxodiferric intermediate during the ferroxidase reaction in fast ferritin mineralization. *Biochemistry* 37(28):9871–9876.
11. Schwartz JK, Liu XS, Tosha T, Theil EC, Solomon EI (2008) Spectroscopic definition of the ferroxidase site in M ferritin: Comparison of binuclear substrate vs cofactor active sites. *J Am Chem Soc* 130(29):9441–9450.
12. Bou-Abdallah F (2010) The iron redox and hydrolysis chemistry of the ferritins. *Biochim Biophys Acta* 1800(8):719–731.
13. Theil EC, Behera RK, Tosha T (2013) Ferritins for chemistry and for life. *Coord Chem Rev* 257(2):579–586.
14. Tosha T, et al. (2012) Ferritin protein nanocage ion channels: Gating by N-terminal extensions. *J Biol Chem* 287(16):13016–13025.
15. Haldar S, Bevers LE, Tosha T, Theil EC (2011) Moving iron through ferritin protein nanocages depends on residues throughout each four α-helix bundle subunit. *J Biol Chem* 286(29):25620–25627.
16. Tosha T, Ng HL, Bhattasali O, Alber T, Theil EC (2010) Moving metal ions through ferritin-protein nanocages from three-fold pores to catalytic sites. *J Am Chem Soc* 132(41):14562–14569.
17. Bertini I, et al. (2012) Structural insights into the ferroxidase site of ferritins from higher eukaryotes. *J Am Chem Soc* 134(14):6169–6176.
18. Masuda T, Goto F, Yoshihara T, Mikami B (2010) Crystal structure of plant ferritin reveals a novel metal binding site that functions as a transit site for metal transfer in ferritin. *J Biol Chem* 285(6):4049–4059.
19. Toussaint L, Bertrand L, Hue L, Crichton RR, Declercq JP (2007) High-resolution X-ray structures of human apoferritin H-chain mutants correlated with their activity and metal-binding sites. *J Mol Biol* 365(2):440–452.
20. Turano P, Lalli D, Felli IC, Theil EC, Bertini I (2010) NMR reveals pathway for ferric mineral precursors to the central cavity of ferritin. *Proc Natl Acad Sci USA* 107(2): 545–550.
21. Rubino JT, Franz KJ (2012) Coordination chemistry of copper proteins: How nature handles a toxic cargo for essential function. *J Inorg Biochem* 107(1):129–143.
22. Savelieff MG, et al. (2008) Experimental evidence for a link among cupredoxins: Red, blue, and purple copper transformations in nitrous oxide reductase. *Proc Natl Acad Sci USA* 105(23):7919–7924.
23. Stefanini S, Desideri A, Vecchini P, Drakenberg T, Chiancone E (1989) Identification of the iron entry channels in apoferritin. Chemical modification and spectroscopic studies. *Biochemistry* 28(1):378–382.
24. Bellapadrona G, Stefanini S, Zamparelli C, Theil EC, Chiancone E (2009) Iron translocation into and out of Listeria innocua Dps and size distribution of the protein-enclosed nanomineral are modulated by the electrostatic gradient at the 3-fold "ferritin-like" pores. *J Biol Chem* 284(28):19101–19109.
25. Haas KL, Franz KJ (2009) Application of metal coordination chemistry to explore and manipulate cell biology. *Chem Rev* 109(10):4921–4960.
26. Mapolelo DT, Zhang B, Naik SG, Huynh BH, Johnson MK (2012) Spectroscopic and functional characterization of iron-bound forms of Azotobacter vinelandii (Nif)IscA. *Biochemistry* 51(41):8056–8070.
27. Cyert MS, Philpott CC (2013) Regulation of cation balance in Saccharomyces cerevisiae. *Genetics* 193(3):677–713.
28. Liu X, Theil EC (2004) Ferritin reactions: Direct identification of the site for the diferric peroxide reaction intermediate. *Proc Natl Acad Sci USA* 101(23):8557–8562.
29. Tosha T, Hasan MR, Theil EC (2008) The ferritin Fe2 site at the diiron catalytic center controls the reaction with O2 in the rapid mineralization pathway. *Proc Natl Acad Sci USA* 105(47):18182–18187.